A New Mixed-Valence Ferrite with a Cubic Structure, $YBaFe_4O_7$: Spin-Glass-Like Behavior

V. Caignaert,*,† A. M. Abakumov,‡ D. Pelloquin,† V. Pralong,† A. Maignan,† G. Van Tendeloo,‡ and B. Raveau†

Laboratoire CRISMAT, UMR 6508, CNRS-ENSICAEN, Université de Caen, 14050 Caen Cedex, France, and EMAT, University of Antwerp, Groenenborgerlaan 171, B-2020 Antwerp, Belgium

Received December 8, 2008. Revised Manuscript Received January 19, 2009

A new mixed-valence ferrite, $YBaFe_4O_7$, has been synthesized. Its unique cubic structure, with $a = 8.9595(2)$ Å, is closely related to that of the hexagonal "114" oxides $YBaCo_4O_7$ and $CaBaFe_4O_7$. It consists of corner-sharing FeO_4 tetrahedra, forming triangular and kagome layers parallel to $(111)_C$. In fact, the $YBaFe_4O_7$ and $CaBaFe_4O_7$ structures can be described as two different "*ccc*" and "*chch*" close packings of $[BaO_3]_\infty$ and $[O_4]_\infty$ layers, respectively, whose tetrahedral cavities are occupied by Fe^{2+}/Fe^{3+} cations. The local structure of $YBaFe_4O_7$ is characterized by a large amount of stacking faults originating from the presence of "hexagonal" layers in the "*ccc*" cubic close-packed $YBaFe_4O_7$ structure. In this way, they belong to the large family of spinels and hexagonal ferrites studied for their magnetic properties. Differently from all the ferrites and especially from $CaBaFe_4O_7$, which are ferrimagnetic, $YBaFe_4O_7$ is an insulating spin glass with $T_g = 50$ K.

Introduction

The numerous studies of strongly correlated electron oxides have shown that a mixed valence of the transition element is necessary for the appearance of their unique properties. It is the case of the Cu(II)−Cu(III) mixed valence in superconducting cuprates,[1,2] of the Mn(III)−Mn(IV) mixed valence in colossal magnetoresistive (CMR) manganites [3,4] and of Co(III)−Co(IV) mixed valence in superconducting[5] and magnetoresistive [6,7] cobaltites. In contrast to these oxides, very few mixed-valence iron oxides have been studied to date, in spite of the very important results previously obtained by many authors on the magnetite Fe_3O_4,[8,9] and on the $LnFe_2O_4$ oxides,[10,11] whose mixed valence Fe(II)−Fe(III) plays a crucial role in the magnetic transitions and charge ordering phenomena. On the basis of these considerations, we have recently explored iron oxides in reduced conditions in order to stabilize the mixed valence Fe(II)−Fe(III), and we discovered a new series of ferrites $Ca_{1-x}Y_xBaFe_4O_7$ with ferrimagnetic properties for $0 \leq x \leq 0.80$.[12] The hexagonal structure of these compounds is similar to that of $LnBaZn_3AlO_7$ first discovered by Müller-Buschbaum et al.[13] and the more recently studied $YBaCo_4O_7$,[14] whose Co(II)−Co(III) mixed valence plays a crucial role in the interesting magnetic properties.[15−18] Bearing in mind these results, we have explored the Ba−Y−Fe−O system, trying to synthesize new Fe(II)−Fe(III) mixed-valence oxides. Here, we report on the new oxide $YBaFe_4O_7$, whose cubic structure is closely related to the hexagonal structure of $CaBaFe_4O_7$ and we show that this oxide exhibits, different from the latter, a spin-glass behavior with $T_g = 50$ K.

Experimental Section

The oxide $YBaFe_4O_7$ was synthesized in two steps, starting from $BaCO_3$, Fe_2O_3 and metallic Fe powder kept in Argon filled glovebox, in order to avoid any hydration and oxidation. First, the precursor $BaFe_2O_4$ was prepared from a mixture of $BaCO_3$ and Fe_2O_3 at 1200 °C for 12 h in air in order to achieve decarbonation. In a second step, a stoichiometric mixture of $BaFe_2O_4$, Y_2O_3, and

* Corresponding author. E-mail: vincent.caignaert@ensicaen.fr.
† Université de Caen.
‡ University of Antwerp.

(1) Bednorz, J. G.; Müller, K. A. *Earlier and Recent Aspects of Superconductivity*; Springer-Verlag: Weinheim, Germany, 1989.
(2) Raveau, B.; Michel, C.; Hervieu, M.; Groult, D. *Crystal Chemistry of High-T_c Superconducting Copper Oxides*; Springer-Verlag: Weinheim, Germany, 1991.
(3) Tokura, Y., Ed. *Colossal Magnetoresistive Oxides*; Gordon and Breach Science Publishers: Amsterdam, 1999.
(4) Rao, C. N. R., Raveau, B., Eds. *Colossal Magnetoresistance, Charge Ordering and Related Properties of Manganese Oxides*; World Scientific: Singapore, 1998.
(5) Takada, K.; Sakurai, H.; Takayama-Muromachi, E.; Izumi, F.; Dilan, R. A.; Saaki, T. *Nature* **2003**, *422*, 53.
(6) Briceno, G.; Chang, H.; Sun, X. D.; Schultz, P. G.; Xiang, X. D. *Science* **1995**, *270*, 273.
(7) Maignan, A.; Martin, C.; Pelloquin, D.; Nguyen, N.; Raveau, B. *J. Solid State Chem.* **1999**, *142*, 247.
(8) (a) Walz, F. *J. Phys.: Condens. Matter* **2002**, *14*, R285. (b) Verwey, E. J. W.; Hayman, P. W. *Physica* **1941**, *8*, 979.
(9) Goodenough, J. B. *Magnetism and the Chemical Bond*, Interscience Monographs on Chemistry, Huntington New-York, 1976.
(10) Yoshii, K.; Ikeda, N.; Nakamura, A. *Physica B* **2006**, *378*, 585.
(11) Yoshii, K.; Ikeda, N.; Matsuo, Y.; Horibe, Y.; Mori, S. *Phys. Rev. B* **2007**, *76*, 024423.
(12) Raveau, B.; Caignaert, V.; Pralong, V.; Pelloquin, D.; Maignan, A. *Chem. Mater.* **2008**, *20*, 6295.
(13) Müller-Buschbaum, H.; Rabbow, C.; Panzer, S. *Z. Naturforsch.* **1997**, *52*, 546.
(14) Valldor, M.; Andersson, A. *Solid State Sci.* **2002**, *4*, 923.
(15) Caignaert, V.; Maignan, A.; Pralong, V.; Hébert, S.; Pelloquin, D. *Solid State Sci.* **2006**, *8*, 1160.
(16) Valldor, M. *Solid State Sci.* **2006**, *8*, 1272.
(17) Maignan, A.; Caignaert, V.; Pelloquin, D.; Hébert, S.; Pralong, V. *Phys. Rev. B* **2006**, *74*, 165110.
(18) Chapon, L. C.; Radaelli, P. G.; Zheng, H.; Mitchell, J. F. *Phys. Rev. B* **2006**, *74*, 172401.

10.1021/cm803312f CCC: $40.75
Published on Web 02/25/2009

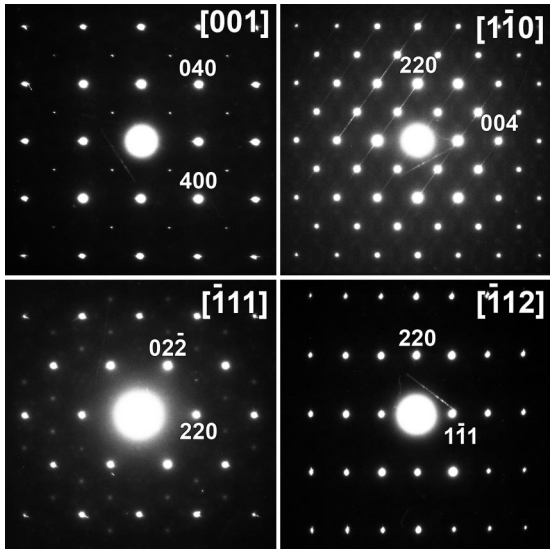

Figure 1. Electron diffraction patterns of $YBaFe_4O_7$.

Fe powder, in the molar ratio 2:1:4, was intimately ground, pressed in the form of bars, and heated in sealed tube under primary vacuum ($\sim 1 \times 10^{-3}$ atm) at 1100 °C for 12 h, in order to fix the oxygen content to "O_7". Finally, the sample was quenched to room temperature. Cerimetric titration led to the oxygen content "$O_{7.08 \pm 0.05}$".

Cell parameters and space group were determined from combined X-ray powder diffraction (XRD) studies and TEM observations. The XRD patterns were registered with a Panalytical X'Pert Pro diffractometer using Cu Kα radiation. TEM observations, in diffraction mode, were carried out with JEOL 2010 and Philips CM20 electron microscopes. The cationic content of numerous crystals was determined by X-ray energy dispersive analysis (EDS) using an INCA analyzer mounted on a Philips CM20 electron microscope. High-resolution images were performed with JEOL 2011 equipped with a field-emission gun (FEG) and JEOL 4000 EX electron microscopes. Simulated HREM images have been calculated using the JEMS and MacTempas softwares.

Magnetization measurements were carried out with a SQUID magnetometer in zero-field-cooling and field-cooling modes ($\mu_0 H = 0.3$ T). A physical property measurement system (PPMS from Quantum Design) was used to measure the ac magnetic susceptibility ($\mu_0 H_{dc} = 0$ T; $\mu_0 H_{ac} = 1 \times 10^{-3}$ T) with the ac/dc magnetic option.

Results and Discussion

The XRD pattern of $YBaFe_4O_7$ reveals the presence of a majority phase with a face centered cubic cell with lattice parameter $a = 8.96$ Å. The volume of the unit cell is twice the volume of the hexagonal $CaBaFe_4O_7$, which leads to four formula units per unit cell ($Z = 4$). The cationic composition, determined by EDS for about 20 crystallites corresponds to the formula "$Y_{0.97(4)}Ba_{1.01(4)}Fe_{4.02(6)}$", in agreement with the nominal composition. Electron diffraction patterns (Figure 1) show that main bright reflections can be indexed with a cubic face centered lattice with $a \approx 9.0$ Å. The $h00$, $h = 2n$ reflections are present on the [1$\bar{1}$0] ED pattern. Recording these reflections upon tilting the crystal around the [001] reciprocal axis reveals that their intensity decreases substantially when multiple diffraction is minimized, but their intensity never vanishes completely. In the [001] ED pattern, where the multiple diffraction conditions for appearance of these reflections are absent, they are still visible as very weak sharp spots. This can be related to the absence of a *d* glide plane in the structure that restricts the possible space groups to *F*23, *Fm*$\bar{3}$, *F*432, *F*$\bar{4}$3*m*, and *Fm*$\bar{3}$*m*. An alternative interpretation of the $h00$, $h = 2n$ spots, as well as of the weak spots at $n/3\{220\}$ positions in the [$\bar{1}$11] ED pattern, is that they result from the intersection of the reciprocal lattice section with the sharp diffuse intensity lines that are clearly visible in the [1$\bar{1}$0] ED pattern. These diffuse intensity lines are parallel to the [111] direction of the cubic lattice and correspond to irregularly spaced planar defects along the {111} planes. It will be shown further by structure refinement and HREM observations that both phenomena (absence of *d*-plane and high amount of stacking faults) contribute to the appearance of the $h00$, $h = 2$n spots.

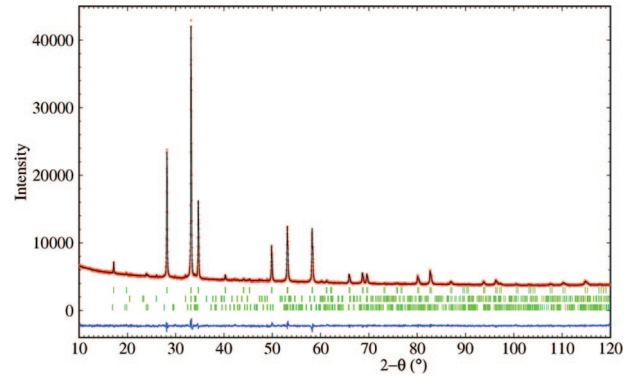

Figure 2. Rietveld refinement of XRPD pattern. Vertical bars mark reflection positions for $YBaFe_4O_7$ (top), $YFeO_3$ (middle), and $BaCO_3$ (bottom) phases.

Table 1. Structural data for $YBaFe_4O_7$

formula	$YBaFe_4O_7$
formula weight	561.64 g/mol
Z	4
cryst syst	cubic
space group	*F*$\bar{4}$3*m* (216)
cell param	$a = 8.9595(2)$ Å
cell volume	719.19(3) Å^3
calcd density	5.195 g/cm^3
χ^2, R_{WP}, R_B	1.78, 11.7%, 4.97%

Table 2. Atomic coordinates for $YBaFe_4O_7$

atom	*x/a*	*y/b*	*z/c*	*B* (Å^2)	position
Y	0	0	0	1.8(5)	4*a*
Ba	3/4	3/4	3/4	1.8(5)	4*d*
Fe	0.3818(5)	0.3818(5)	0.3818(5)	1.8(5)	16*e*
O1	0.7596(23)	0	0	1.8(5)	24*f*
O2	1/4	1/4	1/4	1.8(5)	4*c*

Expectations of an ordered distribution of the Y^{3+} and Ba^{2+} cations and the cationic composition $YBaFe_4O_7$ ($Z = 4$) suggest a space group *F*$\bar{4}$3*m* because it allows the location of Y and Ba atoms on individual sites. The crystal structure determination has been carried out by global optimization in direct space with the program FOX[19] by defining rigid FeO_4 tetrahedra and optimizing their position and orientation. A solution was rapidly obtained leading to five independent sites for Y, Ba, Fe, and O. Once convergence was achieved, the refinement of the crystal

(19) Favre-Nicolin, V.; Cerny, R. *J. Appl. Crystallogr.* **2002**, *35*, 734.

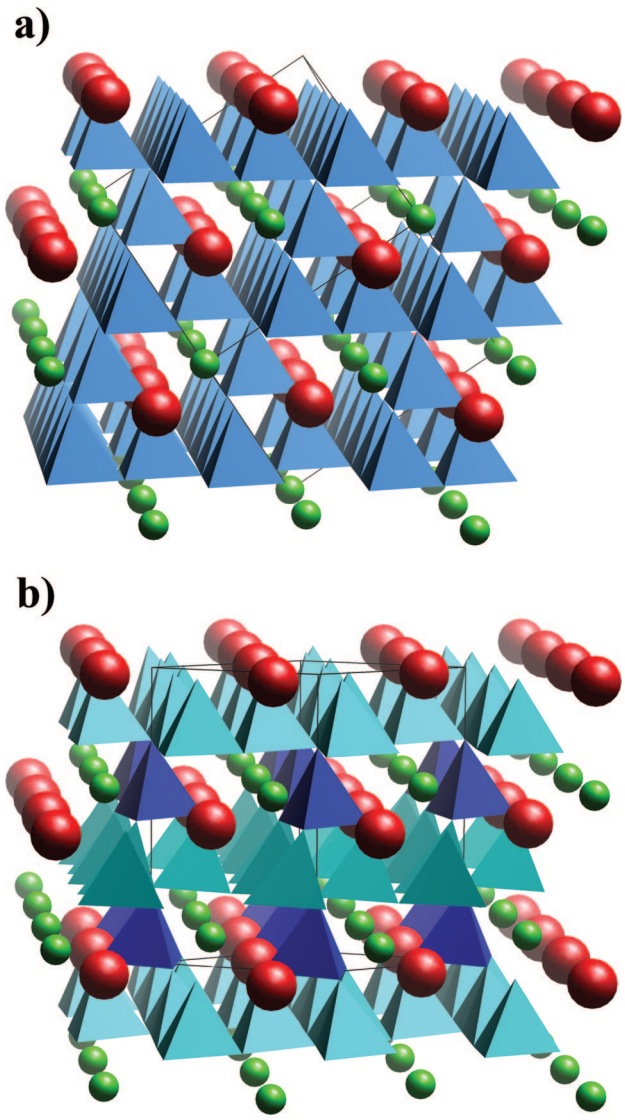

Figure 3. Perspective view for the cubic structure of $YBaFe_4O_7$ nearly along $\langle 111\rangle_C$ (a) and for the hexagonal structure of $CaBaFe_4O_7$ nearly along $\langle 1\bar{1}0\rangle_H$ (b), showing the $[Fe_4O_7]$ framework.

structure parameters was carried out using the FullProf software.[20] Two other phases, detected in the course of the refinement, were taken into account: $YFeO_3$ (6% in mass) and $BaCO_3$ (1% in mass). After the refinement of the three structural parameters for $YBaFe_4O_7$ (x_{Fe}, x_{O1} and an overall thermal factor), the goodness of fit decreases to $\chi^2 = 1.78$, $R_{WP} = 11.7\%$, $R_B = 4.97\%$. The experimental, calculated, and difference XRD patterns are shown in Figure 2. The structural data and atomic parameters are given in Tables 1 and 2, respectively.

Description of the Structure. The cubic structure of $YBaFe_4O_7$ (Figure 3a) is closely related to that of $CaBaFe_4O_7$ (Figure 3b). In both structures, the three-dimensional framework $[Fe_4O_7]_\infty$ consists of corner-sharing FeO_4 tetrahedra and forms two sorts of layers parallel to $(111)_C$ or to $(001)_H$, named kagome (K) and triangular (T), respectively. These layers are stacked along $\langle 111\rangle_C$ or $\langle 001\rangle_H$ in such a way that one kagome layer alternates with one triangular layer. The

(20) Rodriguez-Carvajal, J. *Physica B* **1993**, *192*, 55.

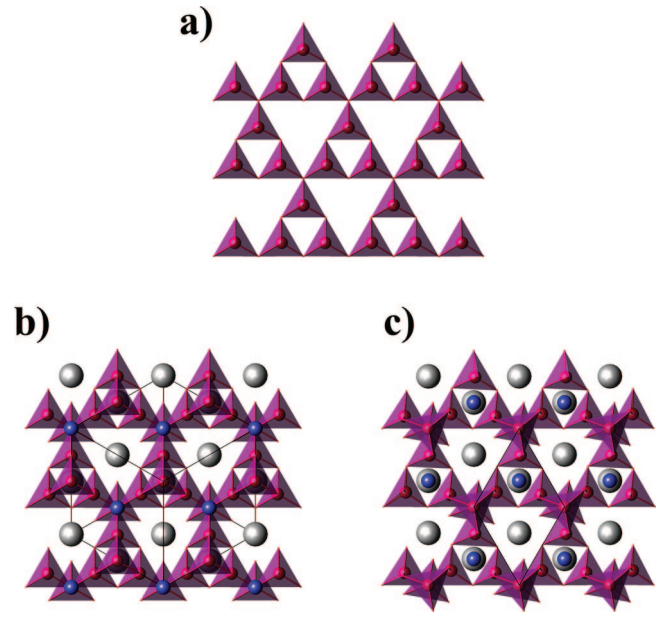

Figure 4. (a) Kagome layers in $YBaFe_4O_7$ and $CaBaFe_4O_7$ and relative positions of the triangular layers that sandwich the latter in (b) $YBaFe_4O_7$ and in (c) $CaBaFe_4O_7$.

geometry of the kagome layers (Figure 4a) is identical in both structures, forming large triangular windows. The two triangular layers which sandwich the kagome layers exhibit also the same geometry in both structures, but their relative positions with respect to the kagome layer are different. In the cubic $YBaFe_4O_7$, the tetrahedra of one triangular layer T_1 are shifted by $a/2$ in the (111) plane with respect to the second triangular layer T_2 (Figure 4b). In contrast, in the hexagonal $CaBaFe_4O_7$ layer, the tetrahedra of the two triangular layers that sandwich one kagome layer are above each other but rotated by about 60°, adopting a staggered configuration (Figure 4c).

Comparing both structures along the $\langle 110\rangle_C$ direction of the cubic $YBaFe_4O_7$ (Figure 5a) and along the $\langle 100\rangle_H$ direction of the hexagonal $CaBaFe_4O_7$ (Figure 5b) clearly shows their relationship. The $[Fe_4O_7]_\infty$ framework forms large triangular tunnels running along $\langle 110\rangle_C$ and $\langle 100\rangle_H$, respectively. Such tunnels are perfectly regular in the cubic phase, whereas they are distorted in the hexagonal oxide. Moreover, the relative positions of the tunnels are different in the two structures. In fact, the cubic $[Fe_4O_7]_\infty$ framework can be deduced from the hexagonal framework of $CaBaFe_4O_7$, by shifting the iron cations in one triangular layer out of two, by b/2 (see arrows in Figure 5b) so that new kagome layers are generated at ~70° from the $(001)_H$ kagome layers The interatomic distances observed for $YBaFe_4O_7$ (table 3) are in perfect agreement with the ionic radii of Y^{3+} in octahedral coordination, and with the average ionic radii of Fe^{3+}/Fe^{2+}, in tetrahedral coordination, imposing a high spin configuration of iron. The YO_6 octahedra are regular with Y−O distances of 2.15 Å, whereas the FeO_4 tetrahedra are elongated with three shorter bonds of 1.96 Å and a longer one of 2.045 Å.

$CaBaFe_4O_7$ and $YBaFe_4O_7$: Close Packed Structures, Related to Perovskites, Hexagonal Ferrites, and Spinels. The large triangular tunnels formed by the FeO_4 tetrahedra are

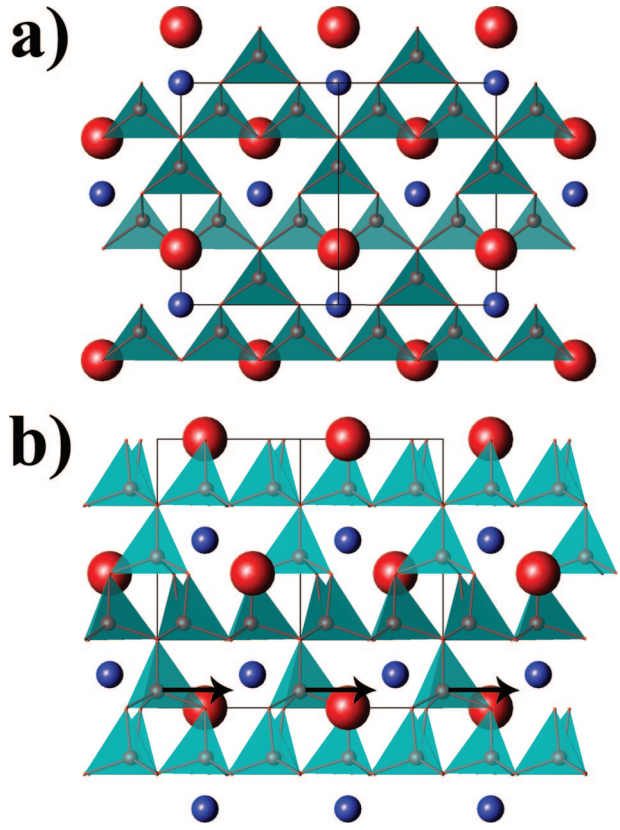

Figure 5. View of the structures of (a) $YBaFe_4O_7$ along $\langle 110\rangle_C$ and (b) $CaBaFe_4O_7$ along $\langle 1\bar{1}0\rangle_H$, showing the large hexagonal tunnels running along those directions.

Table 3. Selected Distances for $YBaFe_4O_7$

bond	distance (Å)
Y−O1	2.15(2) × 6
Ba−O1	3.169(1) × 12
Fe−O1	1.96(1) × 3
Fe−O2	2.045(4) × 1

obstructed by YO_6 and CaO_6 octahedra, so that these two structures should also be described as close-packed structures. In fact, the Ba^{2+} and O^{2-} species form $[BaO_3]_\infty$ hexagonal or slightly distorted hexagonal close packed layers (Figure 6a), similar to those observed for the perovskite $BaTiO_3$. Different from the latter, in those ferrites one BaO_3 layer alternates with one "O_4" hexagonal close packed layer along $[001]_H$ or $\langle 111\rangle_C$. As a consequence, the structures can be described as a cubic close packing of "ABC ABC" (*ccc*) type for $YBaFe_4O_7$ (Figure 6b) and as a close packing of the "ABCB" (*chch*) type for the hexagonal $CaBaFe_4O_7$ (Figure 6c). Such close packings have previously been observed for pure "O_4" anionic layers or pure "BaO_3" layers. The close packing of $YBaFe_4O_7$ can indeed be derived from the close packing of the spinel structure. This can be done by an ordered replacement by Ba atoms of one oxygen atom out of four in half of the "O_4" layers of the "O_8" spinel framework. In a similar way, the close packing of the hexagonal $CaBaFe_4O_7$ corresponds to the 4H — type of the hexagonal $BaCoO_3$ perovskite, where the "BaO_3" layers also form an "ABCB" stacking. In these two different close packings both tetrahedral and octahedral cavities are available for

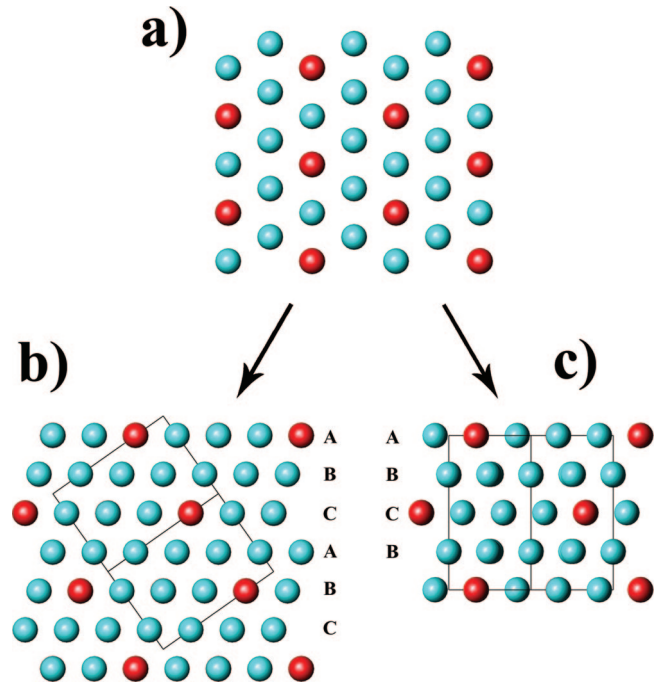

Figure 6. (a) Hexagonal close-packed "BaO_3" layers forming (b) a cubic "ABCABC" close packing with "O_4" layers in $YBaFe_4O_7$ and (c) a hexagonal "ABCB" close packing with "O_4" layers in $CaBaFe_4O_7$.

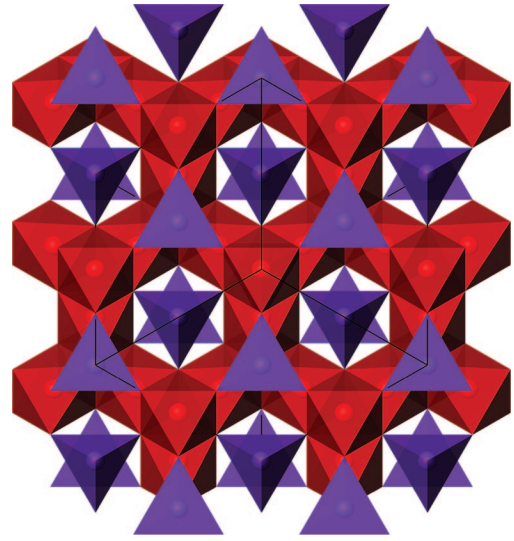

Figure 7. Spinel structure view along κ of three layers: octahedral kagome and two triangular layers.

smaller cations. The $CaBaFe_4O_7$ and $YBaFe_4O_7$ ferrites differ from the pure isotypic "O_4" or "BaO_3" stackings by the fact that their iron cations sit only in tetrahedral cavities, whereas they exhibit both coordinations — tetrahedral and octahedral — in the Fe_3O_4 spinel, and the coordination of the transition element in the hexagonal 4H perovskite is purely octahedral. Moreover, there is a close relationship between the Fe_3O_4 spinel and the cubic $YBaFe_4O_7$; both structures exhibit triangular layers with a similar geometry and kagome layers forming hexagonal windows. However, they differ by the fact that the kagome layers are built up of FeO_6 octahedra in the spinel (Figure 7), whereas they consist of FeO_4 tetrahedra in $YBaFe_4O_7$

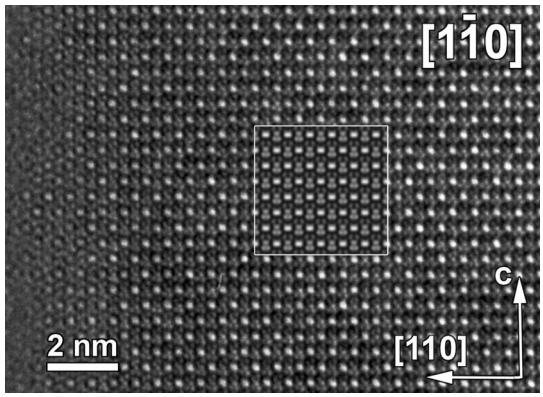

Figure 8. [1$\bar{1}$0] HREM image of $YBaFe_4O_7$. Calculated image is shown as inset: ($\Delta f = -90$ nm, $t = 3.5$ nm).

(Figure 4a).

Finally, the relationship between these two ferrites and the hexagonal ferrites should be emphasized[21] because the latter also contain similar close-packed "BaO_3" layers, associated to the "O_4" hexagonal layers. In this way, $YBaFe_4O_7$ as well as $CaBaFe_4O_7$ can be considered as end-members of the series of hexagonal ferrites, where one "BaO_3" layer alternates with one "O_4" layer, whereas the spinel structure Fe_3O_4 is the other end member, built up of only "O_4" close-packed layers.

HREM Observations. To validate this model, a HREM study has been carried out. Taking into account the structure previously defined, the [1$\bar{1}$0] HREM image provides the most useful structural information. The experimental image shown in Figure 8 has been recorded with a defocus value close to −90 nm. The brightest dots on the image correspond to the projections of the Fe columns in the pseudohexagonal tunnels delimited by 3Ba and 3Y atoms (i.e., in tetrahedra with triangular faces at the "O_4" layers, see structure projection in Figure 5a). Calculated image (inset in Figure 8) based on the refined atomic positions (Table 2) fits well the experimental image contrasts.

The low-magnification [1$\bar{1}$0] HREM image (Figure 9) represents a highly faulted region of the $YBaFe_4O_7$ crystal. The defect planes are parallel to $(111)_c$ and can be divided into two categories. The majority of the planar defects only introduce a sideway displacement of the prominent bright dot patterns by $\pm 1/3$ of interplanar spacing of the $(11\bar{1})_c$ lattice planes. These defects can be classified as antiphase boundaries (APBs). Some planar defects, however (marked by arrows in Figure 9), break the crystal into domains with mirror-related orientation with respect to the $(11\bar{1})_c$ lattice planes. These defects are twin planes. A higher magnification of the twinned region is shown in Figure 10. The positions of brighter dots are associated with the "O_4" layers. By marking the brighter dots by circles in the direction perpendicular to the $(111)_c$ plane one can easily reveal the "ABC ABC" (or *ccc ccc*) stacking of the close packed layers (3 "BaO_3" and 3 "O_4" layers per 3 dots). At the interface, the stacking is violated by the insertion of one "hexagonal"-type "*h*" layer. It is reasonable to assume that the transformation of one "cubic" layer to a "hexagonal" one occurs

(21) Smit, J.; Wijn, H. P. J. *Ferrite*; Philips Technical Library: Eindhoven, The Netherlands, 1960.

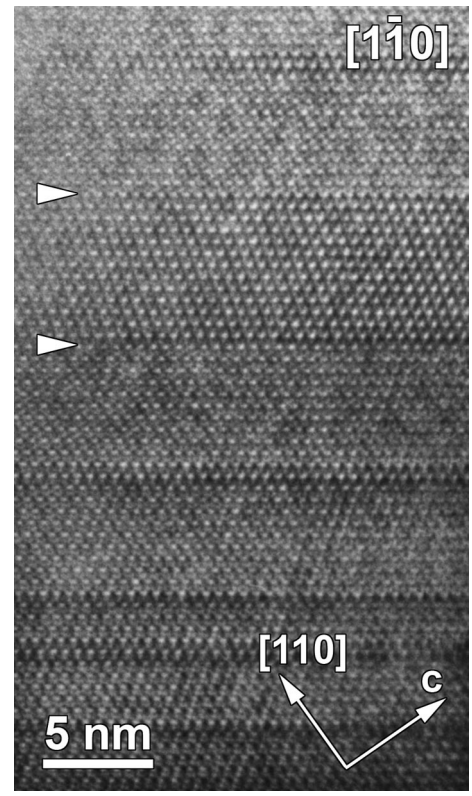

Figure 9. [1$\bar{1}$0] HREM image of $YBaFe_4O_7$ showing a region with high concentration of planar defects.

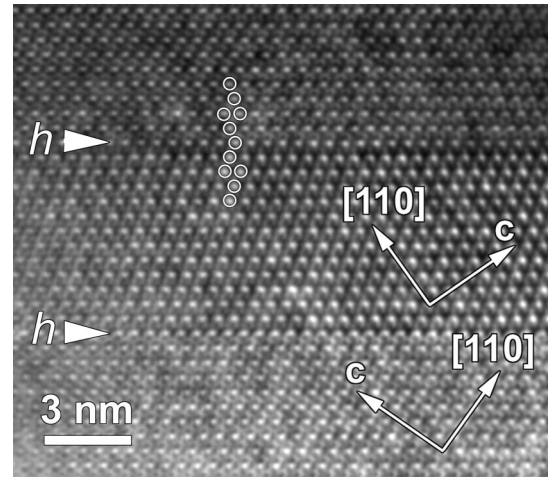

Figure 10. HREM image of YBaFe4O7 showing twin boundaries (the model is in Figure 11a). "Hexagonal" layers are marked with arrows.

according to panels b and c in Figure 6. One of the close-packed "O_4" layers (for example, the top layer in Figure 6b) sandwiching the "BaO_3" layer is rotated over 180° around the $[111]_c$ axis transforming the "BaO_3" layer from "*c*" to "*h*" type. Such transformation results in the formation of 180° rotation twins with $(111)_c$ as a twin plane. In fact, the obtained fragment containing the "hexagonal" layer can be considered as a lamella of the "ABCB ABCB" (*chch*) $CaBaFe_4O_7$-type structure in a matrix of cubic *ccc* close packing of $YBaFe_4O_7$. One can expect that structure relaxation at the "*h*" layer leads to atomic displacements in the "*h*" layers of the $CaBaFe_4O_7$ structure. Taking this hypothesis into account, we propose the twin boundary structure shown

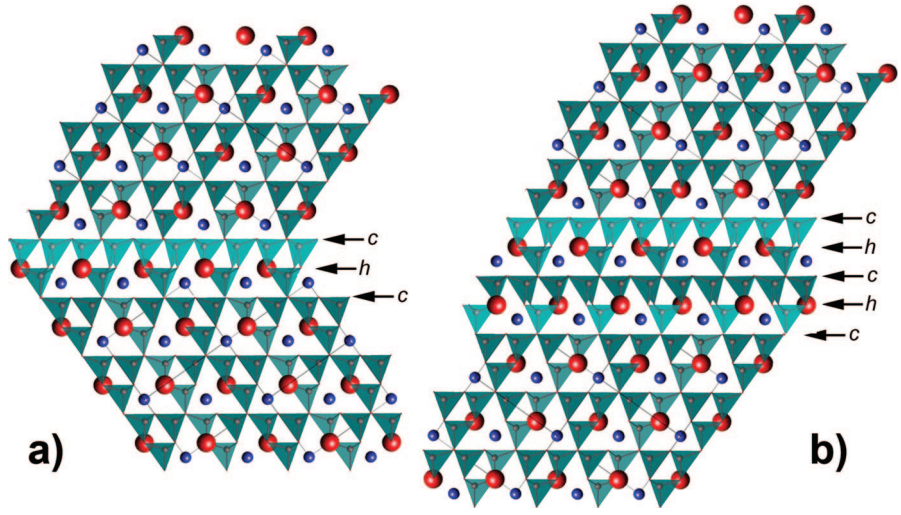

Figure 11. Atomic models of (a) twin boundary and (b) "*chchc*" antiphase boundary in $YBaFe_4O_7$. The "*chc*" and "*chchc*" fragments represent lamellas of the $CaBaFe_4O_7$-type structure.

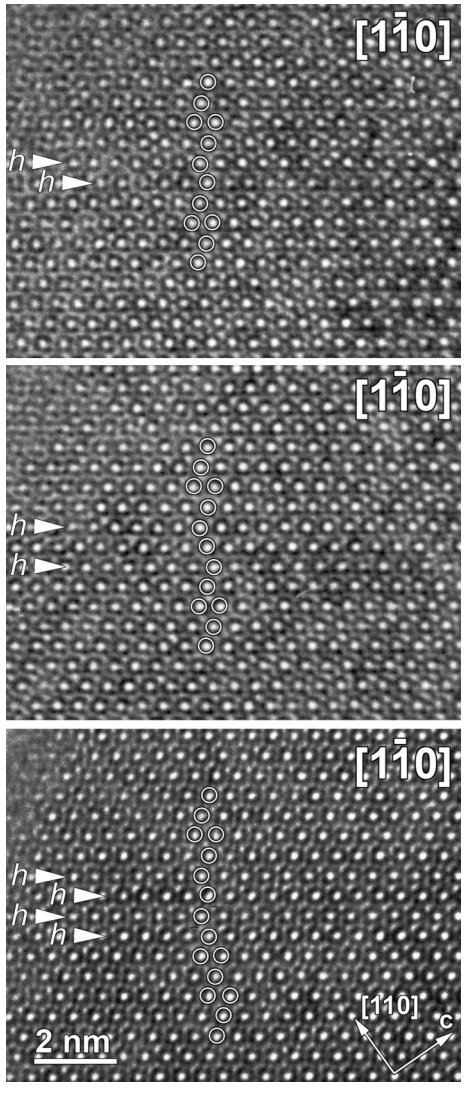

Figure 12. [1$\bar{1}$0] HREM images of $YBaFe_4O_7$ showing different structures of the antiphase boundaries (APBs). From top to bottom: "*chchc*" APB (the model is in Figure 11b); "*chccchc*" APB and "*chchchchc*" APB. "Hexagonal" layers are marked with arrows.

in Figure 11a. Antiphase boundaries arise when an even amount of "*h*" layers are positioned next to each other, so

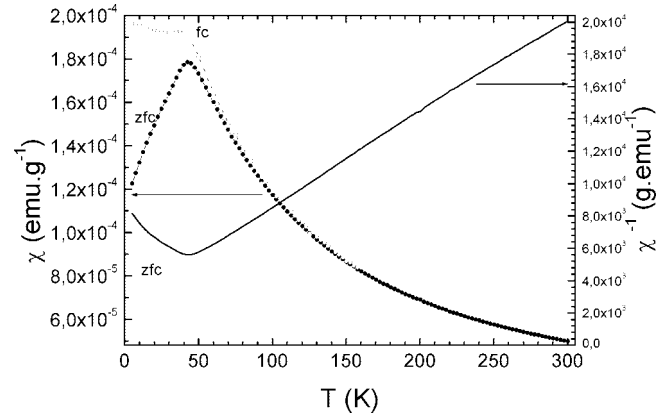

Figure 13. (left *y*-axis) T-dependence of the magnetic susceptibility χ (= *M*/*H*) collected according to zero-field-cooling (ZFC) and field- cooling (FC) processes ($\mu_0 H$ = 0.3 T); (right *y*-axis) corresponding *T*-dependent reciprocal magnetic susceptibility (χ^{-1}) from ZFC $\chi(T)$ curve.

that the associated rotations are mutually compensated. We have observed that the APBs are formed by different stacking sequences. The simplest one is "....*chchc*..." (Figure 12, top), which in fact represents a lamella of the $CaBaFe_4O_7$ structure of one unit cell width (see Figure 11b). The HREM images of the APBs with different structures are shown in Figure 12.

Magnetic Properties. For $YBaFe_4O_7$, the T-dependence of the magnetic susceptibility (χ = M/H) measured in 0.3T (Figure 13) strongly differs from the ferrimagnetic-like behavior of $CaBaFe_4O_7$[12] whose T_C is 250 K. For $YBaFe_4O_7$ the reciprocal magnetic susceptibility ($\chi^{-1}(T)$; Figure 13) reveals a paramagnetic regime extending in the *T* range of 50 K < $T \leq$ 300 K. The Curie−Weiss law [$\chi = C/(T + \theta)$] fits the curve leading to a paramagnetic effective magnetic moment per iron cation μ_{eff} = 4.45 μ_B, i.e., a slightly lower value than expected for high spin Fe^{2+}(S = 2) and Fe^{3+}(S = 5/2) in a 3:1 ratio (μ_{eff} = 5.2 μ_B). The Curie−Weiss temperature obtained by extrapolation of the linear $\chi^{-1}(T)$ region leads to θ = −22K, indicating the existence of antiferromagnetic fluctuations at high temperature in this oxide. Furthermore, the $\chi(T)$ ZFC curve shows a maximum at 45 K with a cusplike shape suggesting the existence of a

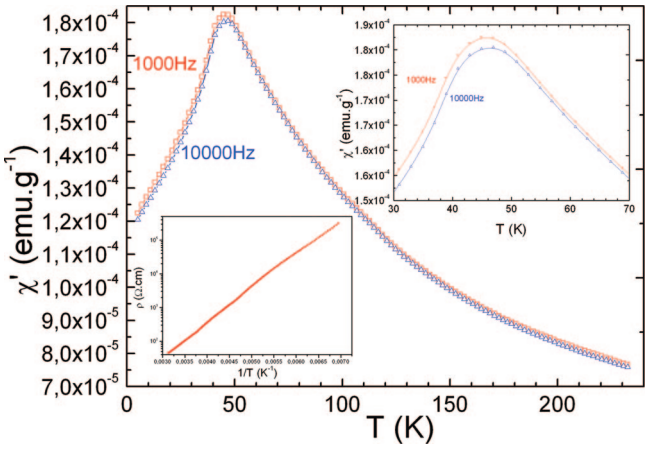

Figure 14. *T*-dependence of the real part of the ac-χ measured at 2 frequencies for the excitation magnetic field ($\mu_0 H = 1 \times 10^{-3}$ T). An enlargement in the *T* region of the χ' maximum is given in the upper right region. The T^{-1} dependence of the electrical resistivity ρ is given at the bottom left inset.

magnetic frustration or an antiferromagnetic transition at that temperature. The comparison of the ZFC and FC curves reveals a quasi *T*-independent FC curve below 45 K, both ZFC and FC curves merging above that temperature. Such curves are strongly reminiscent of those found in spin glasses. To probe for this kind of behavior, ac-χ measurements have been performed. The data collected for two frequencies ($f = 1 \times 10^3$, 1×10^4 Hz) confirm the existence of a cusp-like feature peaking at the $T_g \approx 45$ K (Figure 14). The enlargement around this maximum (Inset of Figure 14) shows a slight increase in T_g by about ~1 K as *f* increases. Such a behavior confirms the existence of a spin-glass-like behavior in $YBaFe_4O_7$ with $T_g = 45$ K. Neutron diffraction is now required in order to test the lack of long-range magnetic ordering below T_g.

This magnetic behavior for $YBaFe_4O_7$ demonstrates that its magnetic structure tends to be frustrated down to low temperature in marked contrast to the behavior of the ferrimagnetic $CaBaFe_4O_7$. This could be explained by either the less frustrated magnetic structure of the latter or by their different mean iron oxidations states, $\upsilon_{Fe} = +2.25$ and $\upsilon_{Fe} = +2.50$ for $YBaFe_4O_7$ and $CaBaFe_4O_7$, respectively. To test the existence of a possible Fe mixed-valency, we also carried out transport measurements. The electrical resistivity ρ is found to be large, with $\rho_{300K} \approx 50\ \Omega$ cm (inset of Figure 14). Its *T* dependence exhibits a thermally activated behavior with activation energy of 1.07 eV, pointing toward a lack of electronic delocalization between the Fe^{2+} and Fe^{3+} species. Accordingly, this phase belongs to the class of insulating spin glasses, because its resistivity at T_g is well beyond $1 \times 10^6\ \Omega$ cm. Considering this insulating nature, the origin of the magnetic coupling is by superexchange. The randomness of the Fe−O−Fe magnetic interactions in this compound, together with the geometric frustration coming from the triangular and kagome sublattices, might be the important factors responsible for this spin-glass behavior.

Conclusion

The mixed-valence ferrite $YBaFe_4O_7$ can be described as a new member of the "114" family of cobaltites and more recently of ferrites, studied for their attractive magnetic and transport properties. In spite of its close structural relationship with these oxides, it differs from the latter by its unique cubic symmetry, offering for iron only one crystallographic site. It is this feature, with the triangular geometry of the structure which is at the origin of the magnetic frustration observed for this compound, similarly to what is observed for pyrochlores. In fact, all the oxides of the "114" family can be regarded as cubic or hexagonal close packings of "BaO_3" and "O_4" layers, similarly to the hexagonal ferrites and to the spinels. They differ from the latter by the fact that the coordination of iron is exclusively tetrahedral. Such structural relationship suggests that it should be possible to generate many other structures by tuning the cations to the octahedral and tetrahedral sites formed by various stackings of "BaO_3" and "O_4" layers. A neutron diffraction investigation will be necessary to better understand the magnetic behavior of this phase.

Acknowledgment. The authors acknowledge financial support of the European Union under the Framework 6 program under a contract for an Integrated Infrastructure Initiative (Reference 026019 ESTEEM), under the Network of Excellence (Reference 500159-2), and under the Marie-Curie fellowship program (Reference MEST-CT-2004-514237 NOVELOX).

CM803312F